Technoeconomic analysis of internal combustion engine – organic Rankine cycle systems for combined heat and power in energy-intensive buildings

Michael C. Simpson[a,*], Maria Anna Chatzopoulou[a], Oyeniyi A. Oyewunmi[a], Niccolo Le Brun[a], Paul Sapin[a], Christos N. Markides[a]

[a] *Clean Energy Processes (CEP) Laboratory, Department of Chemical Engineering, Imperial College London, South Kensington Campus, London SW7 2AZ, United Kingdom.*

Abstract

For buildings with low heat-to-power demand ratios, installation of internal combustion engines (ICEs) for combined heat and power (CHP) results in large amounts of unused heat. In the UK, such installations risk being ineligible for the CHP Quality Assurance (CHPQA) programme and incurring additional levies. A technoeconomic optimisation of small-scale organic Rankine cycle (ORC) engines is performed, in which the ORC engines recover heat from the ICE exhaust gases to increase the total efficiency and meet CHPQA requirements. Two competing system configurations are assessed. In the first, the ORC engine also recovers heat from the CHP-ICE jacket water to generate additional power. In the second, the ORC engine operates at a higher condensing temperature, which prohibits jacket-water heat recovery but allows heat from the condenser to be delivered to the building. When optimised for minimum specific investment cost, the first configuration is initially found to deliver 20% more power (25.8 kW) at design conditions, and a minimum specific investment cost (1600 £/kW) that is 8% lower than the second configuration. However, the first configuration leads to less heat from the CHP-ICE being supplied to the building, increasing the cost of meeting the heat demand. By establishing part-load performance curves for both the CHP-ICE and ORC engines, the economic benefits from realistic operation can be evaluated. The present study goes beyond previous work by testing the configurations against a comprehensive database of real historical electricity and heating demand for thirty energy-intensive buildings at half-hour resolution. The discounted payback period for the second configuration is found to lie between 3.5 and 7.5 years for all of the buildings considered, while the first configuration is seen to recoup its costs for only 23% of the buildings. The broad applicability of the second configuration offers attractive opportunities to increase manufacturing volumes and reduce unit costs. The findings are relevant to a range of buildings with heat-to-power demand ratios from 20% to 100%.

Keywords: CHP, combined heat and power, cogeneration, high efficiency, ORC, organic Rankine cycle, condenser heat rejection

The short version of this paper was presented at ICAE2018, Aug 22-25, Hong Kong. This paper is a substantial extension of the short version of the conference paper [1].

*Corresponding author
Email address: m.simpson16@imperial.ac.uk (Michael C. Simpson)

List of Acronyms

CAMD computer-aided molecular design

CAPEX capital expenditure

CEPCI Chemical Engineering Plant Cost Index

CHP combined heat and power

CHPQA Combined Heat and Power Quality Assurance

DPP discounted payback period

HX heat exchanger

ICE internal combustion engine

NPV net present value

OPEX operational expenditure

ORC organic Rankine cycle

QI quality index

SAFT statistical associating fluid theory

SIC specific investment cost

1. Introduction

Interest in distributed combined heat and power (CHP) generation has been steadily growing, due to the higher overall efficiency of such systems relative to the separate provision of heat and power [2]. This solution allows a lower overall energy use and lower costs for the user, as well as a lower environmental impact of the system compared to traditional heating and centralised power generation systems, which has led many energy-intensive users to consider the adoption of cogeneration systems.

Large supermarket chains, which face high electricity demands for refrigeration in their many stores and distribution centres, have shown a particular interest in using CHP systems to manage energy costs. Typically, small-to-medium scale CHP systems consist of an internal combustion engine (ICE) coupled with a generator for electricity production. These systems deliver electricity and heat in roughly equal proportions. However, the buildings in question typically have a low heat-to-power ratio, meaning electricity demand far exceeds the demand for heat, resulting in large quantities of unused heat. The imbalance reduces the overall system efficiency and leads to a longer payback period.

In the UK, CHP installations are assessed against a minimum efficiency standard as part of the CHP Quality Assurance (CHPQA) programme [3]. Natural gas installations with an electrical output below 1 MW are assessed using the formula $\mathrm{QI} = 249\eta_\mathrm{p} + 113\eta_\mathrm{h}$, where QI is the quality index, η_p is the electrical efficiency and η_h is the heat efficiency, defined as the useful electrical and heat output respectively per unit of fuel energy input over the course of a year of operation. CHP plants need to demonstrate an electrical efficiency of greater than 20% to qualify, and existing installations are also expected to achieve a QI above 100, while new schemes must achieve a higher QI of 105. For example, a new scheme for a CHP-ICE producing 500 kW of electricity with an average electrical efficiency of 35% and an average heat-to-power ratio of 1.06 would need to make use of at least 42% of the delivered heat. Installations which fail to meet this standard face additional levies and reduced capital allowances, further lowering the project returns.

A technology with the potential to address this problem is the organic Rankine cycle (ORC) engine, which provides an effective means of generating electricity from renewable or waste heat at lower temperatures and/or smaller scales than is possible with conventional power generation [4]. There is a broad literature of studies aiming to optimise the thermodynamic performance of ORC systems for a range of heat sources including, among others, solar-driven ORC engines [5, 6], geothermal applications [7] and waste-heat recovery [8], while the use of computer-aided molecular design (CAMD) approaches based on statistical associating fluid theory (SAFT) have also been shown to lead to suggestions for improved ORC engine performance and working fluid design [9, 10, 11]. In bottoming-cycle configuration, the ORC engine is able to convert the unused heat into additional power generation, driving up the overall efficiency and achieving compliance with the CHPQA standard.

While thermodynamic optimisation and technical feasibility are at the core of the development of ORC systems, a critical factor for their wider deployment is their capital expenditure (CAPEX), and operational and maintenance expenditure (OPEX). The amount of literature publicly available on costs of actual ORC systems is limited. In the absence of actual project cost data, obtaining credible estimates of the ORC system cost requires suitable sizing and costing of the individual system components. These estimates form the basis of the cost calculations to be undertaken when evaluating the financial viability of ORC engine deployment. This approach was followed in White et al. [12] where both the working-fluid design and the thermoeconomic assessment of ORC systems in waste-heat recovery applications was carried out, and in van Kleef et al. [13] where the problem of working-fluid design and thermo-economic optimisation was approached via multi-objective computer-aided molecular design techniques. In both works, individual ORC system components were sized and costed using available data and correlations from various sources.

Lecompte et al. [14] optimised an ORC system for minimum specific investment cost (SIC) while recovering heat from the jacket-water circuit of a CHP engine. For the system costing, the authors used cost correlations based on actual component prices in the Belgian market. Depending on the working fluid and the heat-source conditions, the SIC of the ORC engine varied between 2450 – 2600 £/kW. A technoeconomic analysis of a transcritical dual loop ORC engine recovering heat from an ICE was also performed by Yu et

al. [15]. The authors used the module costing technique for the equipment costing as provided by Turton [16]. Results indicate that discounted payback period (DPP) for the ORC engine varies between 7 and 15 years, depending on the working fluid and pressure levels in the system. Braimakis et al. [17] reported SICs for high-temperature waste heat recovery of 900 – 3000 £/kW, using the cost correlations from Peters et al. [18].

This work focuses on the technoeconomic optimisation of small-scale ORC engines, suitable for use in CHP applications when recovering heat from ICEs. Previous studies have assessed the thermodynamic performance of systems using heat from both jacket water and exhaust gases, but this study goes beyond the existing literature to investigate the economic merits of jacket-water preheating and heat recovery from the ORC engine condenser for a large number of different buildings. A comprehensive database of recorded electricity and heating demand for thirty buildings was obtained from a major UK supermarket chain. Drawing on this highly relevant data, the CHP-ORC systems under consideration are tested at both design and part-load conditions in annual simulations, thereby rigorously evaluating their economic benefits.

The aim of the study is twofold: i) to investigate how system configurations with either jacket-water preheating or condenser heat recovery affect the ORC engine output for a range of working fluids, when optimising for maximum power or for minimum SIC; and ii) to study the effect of these two strategies on running costs over the life of a project, including part-load operation. This allows us to identify how decisions about the ORC system design and sizing influence the overall financial viability of the project, accounting for both the investment and running costs of the system. The screening-phase design tool developed can be used to assess the attractiveness of the chosen cycle architecture and operating strategies early in the design process for a CHP-ORC engine installation, while the subsequent time-resolved simulations offer an in-depth look at project returns, and how they vary from building to building for each ORC system design.

At present, small-scale ORC systems are manufactured in very low volumes, with each customised to the particular application, thereby incurring the additional costs associated with such activities. A design that successfully meets the needs of a range of energy-intensive buildings could be of significant interest to large supermarket chains, amongst others, and would present an opportunity to reduce unit costs by achieving economies of scale through larger-volume manufacturing runs.

2. Methodology

The ORC engines investigated in this work are designed to recover heat from three stationary CHP-ICE engines, designated by the manufacturer as: E210, E375 and E500, where the number gives the approximate electrical output power of the ICE in kilowatt. The heat available from the jacket water and exhaust gas for each engine are obtained from the manufacturer's datasheets [19]. The exhaust gas leaves the CHP-ICE at 480 – 570 °C when the ICE is operating at full load, while the jacket water is delivered at 90 °C. The building hot water supply is fixed at 70 °C. The ORC system configurations are chosen to suit an application where the electrical demand exceeds the thermal demand, i.e., where a potential exists to convert excess heat into electricity. Two configurations are proposed, as indicated in Fig. 1. The schematics have been simplified for

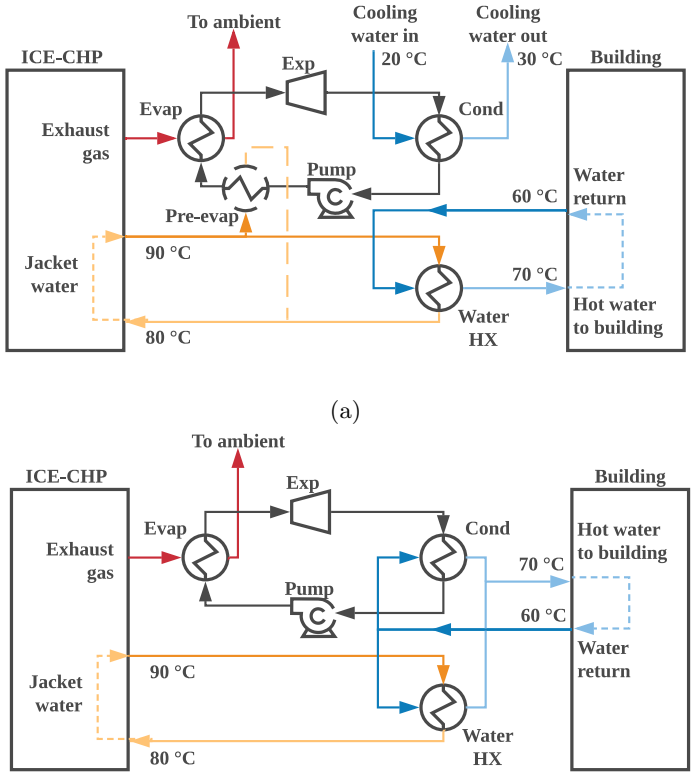

Figure 1: Schematics showing CHP, ORC engine and building in: (a) Configuration 1, with jacket water used to preheat the ORC working fluid before the evaporator and heat rejection from the ORC engine condenser to cooling water, and (b) Configuration 2, with ORC heat rejection to the building hot water supply. The dashed line connecting the pre-evaporator in (a) is used to denote that only part of the jacket water is used for the preheating of the ORC working fluid.

clarity, with water pumps and valves omitted. In both configurations, the ORC engine takes heat directly from the exhaust gas stream. There is no direct heat supply from the ICE exhaust gas to the building in either case. More advanced arrangements are possible in which control valves are used to bypass the ORC engine and divert the exhaust gas flow to a second heat exchanger for additional water heating if needed, but these are beyond the scope of the present study.

In Configuration 1, the ORC system also uses a proportion of the jacket water for preheating (through the heat exchanger labelled 'Pre-evap' in Fig. 1a). This configuration allows (partial) heat recovery from both streams, while using the exhaust gas to evaporate and superheat the working fluid. The amount of heat taken from the water is varied according to the cycle optimisation for each working fluid. The remainder of the jacket water is used to deliver heat to the building. In Configuration 1, cooling water enters the condenser at 20 °C and absorbs heat from the working fluid. The flow rate of water is varied such that the cooling water leaves the condenser at a temperature of 30 °C.

In Configuration 2, the ORC engine only recovers heat from the exhaust gas stream. The jacket water is used exclusively for the building heating. Furthermore, the condensing temperature of the ORC engine is

increased, such that heat from the condenser can then be used to deliver additional hot water to the building. This configuration therefore permits almost all of the CHP-ICE heat to be delivered to the building, but reduces the temperature difference for the ORC to exploit. The merits of this approach have been considered for large-scale installations by Oyewunmi et al. [20].

The following sections detail the ORC engine modelling approach, including heat exchangers and the expander at design and off-design conditions as well as the costing methods used. The application parameters and financial metrics used are provided in Section 2.2. The design process, split into a screening phase with multiple working fluids, and a detailed simulation phase, is described in Section 2.3, leading to an economic analysis of each ORC engine configuration subject to building-specific heat and power demands for a set of thirty buildings.

2.1. Organic Rankine cycle (ORC) model

A non-recuperative sub-critical ORC model has been developed in MATLAB, with fluid properties obtained from REFPROP [21]. An optimisation is carried out according to the methodology outlined by Oyewunmi et al [7, 22], extending the work of Vaja and Gambarotta [23]. The efficiency of the pump is set to 65%, while that of the expander is initially fixed at 70% for the preliminary design study, but is modelled in detail for the subsequent analysis. Both design-point and part-load operation are considered.

2.1.1. Heat exchanger modelling

Counter-flow tube-in-tube heat exchanger (HX) designs are selected for the evaporator and the condenser units, for their simple construction and low cost. The convective heat transfer in the single-phase zones is estimated using the Dittus-Boelter correlation [24], as the flow is turbulent. The asymptotic Chen-Zuber Nusselt number correlation [25, 26] is used to account for both the nucleate and convective boiling contributions in the two-phase zone of the evaporator, while the Shah correlation [27] for combined shear- and gravity-driven phenomena is used for the condenser. A single-stream configuration is modelled, and pipe bends are not accounted for explicitly. Further details on the HX sizing and modelling approaches can be found in Chatzopoulou et al. [28].

Another important factor for the design of HXs is the pressure drop experienced by the working fluid. In direct-fired evaporators recovering heat from ICE exhaust-gas streams, the evaporator HX design should minimise the additional back-pressure added to the engine. In this work, the correlation described in Chatzopoulou et al. [29] for pressure drop for flows in tubes is used, drawing on work by Chisholm [26] for the two-phase flows, based on the Reynolds numbers of the two-phase, liquid-only and gas-only flows.

Initial sizing of the HXs is performed to achieve the required inlet and exit conditions, as specified by means of a maximum power or minimum SIC cycle optimisation. A minimum approach temperature of 10 K is used to limit the maximum size of the HXs during the maximum power optimisation. The single-phase and two-phase sections of each heat exchanger are discretised into elements and the corresponding local Nusselt numbers, Reynolds numbers, heat transfer coefficients and pressure drops are calculated. The heat transfer

in each element of a single- or two-phase section is assumed to be equal, and the area for each element is calculated. The overall geometry of the HX is iteratively refined to achieve the required heat transfer rate while also meeting the pressure drop constraint, thus producing the area of each section and hence the total heat transfer area.

For part-load HX modelling, the same fundamental approach is used, but the geometry and total heat transfer area for each HX is constrained to equal that of the initial design, as part of the operating point optimisation. Operating points which cannot be achieved with the specified heat transfer areas are determined to be infeasible during the optimisation. This approach ensures that the same HXs are being simulated at part-load operation as at design conditions.

2.1.2. Expander modelling

The expansion machine is a key component of the system, as the overall performance of the ORC engine is largely influenced by the choice and design of the expander unit. The choice of the expander type is typically guided by the scale of the system in question. For large systems, delivering 100s of kW, turbines are the default choice, while scroll expanders are commonly employed in micro- and small-scale systems, i.e., in the 1–10 kW range [30]. In the intermediate range, screw and reciprocating-piston expanders are favoured for their low rotational speeds and robust off-design performance. Of the two, a piston expander has been selected in this study for its higher pressure-ratio capabilities per stage, which is advantageous for high-temperature heat sources such as the exhaust gases considered here.

Simplifying assumptions around expander performance are commonly made in early-stage ORC design studies, for example by specifying a fixed isentropic efficiency for the expander. In reality, the peak isentropic efficiency of the piston expander is a function of the operating conditions [31], and so care is required to avoid operating points that unduly constrain the efficiency achievable in practice by the expander. The assumption of fixed expander isentropic efficiency is therefore adopted for the screening phase, but is subsequently refined for the detailed simulation.

For a more detailed prediction of the expander performance, a dynamic lumped-mass model of a reciprocating-piston expander is employed. The model, previously described by Sapin et al. [32], has also been developed in MATLAB and solves the mass and energy balance equations for the gas in the expansion-cylinder space at each timestep. By capturing the major loss mechanisms, the model provides a realistic estimate for the performance that could be achieved by a device under the specified operating conditions. These loss mechanisms consist of valve throttling losses, friction, heat transfer and mass leakage past the piston rings. Valve losses are modelled using 1-D compressible flow relations with a discharge coefficient [33], while friction losses are estimated based on measurements from motored diesel engines [34]. Heat transfer calculations are made using the complex Nusselt number correlation provided by Lekic [35]. Mass leakage past the piston rings is modelled by tracking the mass accumulation in the crevice between the piston rings under the assumption of isentropic flow [36]. The predictions of the model have been validated in gas-spring configuration by experiment and found to agree well [32].

The expander model is used to identify the optimal design for the chosen design point, selecting the device geometry and valve timings by means of a surrogate model-based optimisation. The optimisation is carried out to maximise the expander power output for a given full-load operating point and mass flow rate. A four-cylinder piston expander architecture is specified in advance, with each cylinder having a volume of 0.3 litres at bottom dead centre, in line with commercially-available piston compressor designs of similar power ratings. Subject to the fixed cylinder-volume constraint, the bore, stroke length and clearance height are allowed to vary, along with the inlet and exhaust valve opening durations and diameters. The expander is assumed to operate at a fixed rotational speed of 1500 RPM.

The open-source MatSuMoTo toolbox for surrogate model-based optimisation, developed by Müller [37], is used to reduce the number of lumped-mass model evaluations required and thus reduce the overall computation time, by fitting surrogate models to the simulation outputs that can be evaluated rapidly. Two surrogate models are used in parallel: one for the isentropic efficiency of the expander, and another for the mass flow rate, in order to prioritise expander designs that deliver the design mass flow. The chosen surrogate models employ a radial-basis-function interpolant with cubic splines.

An iterative approach is followed during the surrogate model-based optimisation. A set of evaluations of the full lumped-mass model are carried out and the chosen surrogate models are fitted to these points. The use of radial basis functions allows a surrogate which is an exact interpolant for the evaluated points, with zero deviation at those locations. By rapidly optimising over the surfaces, promising locations for further evaluations of the full model are identified, thereby avoiding time spent evaluating many points far from the optimal design. When the new evaluations of the full model are complete, the fitted surfaces are updated and the process repeats until convergence on the optimum design is achieved. It is worth noting that, in each set of iterations, further points are sampled at random throughout the design space as well as at the promising locations, to ensure that the fitted surface reflects the underlying full model, and to limit the chances of missing a global optimum by focusing only on a local optimum. The optimisation is considered to have converged when five sets of five consecutive iterations of the sampling and evaluating sequence are all found to result in improvements of less than 0.1%. After each set without an improvement, the sampling radius is reduced to focus the search further. The normalised root-mean-square deviation between the final surrogate models and the full model is found to be less than 11% for the isentropic efficiency, and 6% for the mass flow rate, measured using a leave-one-out cross-validation approach. While these deviations mean that the optimum design found using the surrogate models is an approximation to the true optimum, the performance of the identified design is obtained directly from the lumped-mass model, ensuring that the subsequent simulations are physically meaningful.

Once the optimal expander design for the chosen full-load operating point has been determined, the lumped-mass model is used a second time to explore its part-load performance. An expander performance map is generated for use in the part-load study, by simulating the same device at a range of operating conditions. The geometry and valve timings remain fixed at their design values throughout these part-load simulations.

2.1.3. System costing

The cost correlations used in this study are obtained by collating manufacturers' technical datasheets and price lists for the key system components. The evaporator and condenser unit correlations are based on costs for stainless-steel tube-in-tube HXs obtained from Seider et al. [38]. To obtain the piston-expander unit cost, the cost of piston compressors for refrigeration is used as a first point of reference, as provided by the manufacturer AREA Cooling Solutions [39]. The cost correlation provided by Seider et al. [38] is used for the centrifugal pump. The costs are converted into present values using the Chemical Engineering Plant Cost Index (CEPCI). In addition to the hardware costs, several further cost components are required to estimate the total project capital expenditure. These include site preparation, service facilities, contingencies and startup costs in line with Guthrie [16], resulting in a total project CAPEX 30% greater than the capital expenditure on hardware alone.

2.2. Application parameters and financial metrics

The following assumptions (presented in Table 1) are made to model the project economics of the ORC engines, taking into account the building demand for heat and power. The CHP-ICE is initially assumed to deliver heat and power equivalent to running at design (full-load) conditions for 85% of the year for the screening phase, but is modelled on a time-resolved part-load basis in the rest of the analysis. When the CHP-ICE is active, heat can be made available to the ORC system.

Table 1: Assumptions used to estimate financial metrics.

Parameter	Value	Parameter	Value
Discount rate (%)	5	O&M (% of CAPEX)	5
Electricity price (£/kWh)	0.12	Load factor (%)	85
Gas price (£/kWh)	0.03	Project duration (years)	20

The merits of each ORC engine and working fluid combination are assessed using multiple metrics. The primary metric is the discounted payback period, commonly chosen for its simplicity and ease of use. The DPP measures the time taken to repay the initial investment, taking into account the time value of money by discounting future cash flows. The net present value (NPV) of each ORC engine project is also calculated, according to the standard formulation.

2.3. Design process

The process of selecting a design point and working fluid, assessing thermodynamic and thermoeconomic performance, and analysing economic benefits over a year favours a staged approach in order to manage the large number of parameters present. In the current work, the following steps are followed, for Configurations 1 and 2:

1. *Screening phase and working point selection*: the ORC engine is optimised for maximum power and minimum specific investment cost in turn as a screening phase for a range of working fluids, at a design point corresponding to full-load operation of the CHP-ICE.
2. *Application fit and working fluid selection*: the fit of the ORC engine performance to the application is assessed using a simplified heating demand model and a candidate working fluid is selected.
3. *Detailed ORC engine design*: a detailed ORC system is designed for the best-performing working fluid.
4. *Part-load simulation*: a part-load simulation is carried out to establish how the ORC engine performs away from its design point.
5. *Application-specific ORC engine performance*: the economic benefits of the detailed ORC model with part-load performance are assessed using application-specific time-resolved electricity and heat demand data.

Each of these steps are elaborated upon in turn in the following sections.

2.3.1. Screening phase and working point selection

Three different CHP engines are considered as heat sources at this stage, before down-selecting to the most suitable ICE for the application. The ORC engine working point is proposed by means of a maximum power or minimum SIC cycle optimisation. A fixed isentropic efficiency of 70% is used to obtain an initial design point for the expander. Considering both thermodynamic and thermoeconomic optimisation enables a better understanding of the trade-offs made between electrical output and system cost. In the former, the objective function to be maximised is the net power output from the ORC system, $\dot{W}_{\mathrm{net}}$, while in the latter, the specific investment cost is minimised, subject to the following constraints:

$$\begin{aligned} \min_{P_{\mathrm{evap}},\, P_{\mathrm{cond}},\, d_{\mathrm{SH}},\, \dot{m}_{\mathrm{wf}},\, f_{\mathrm{JW}}} \quad & -\dot{W}_{\mathrm{net}} \text{ or } SIC & \\ \text{subject to:} \quad & P_{\mathrm{cond}} \leq P_{\mathrm{evap}} \leq 0.85 P_{\mathrm{crit}} & T_3 \leq T_{\mathrm{max}} \\ & 0 \leq f_{\mathrm{JW}} \leq 1 & T_4 \geq T_{4\mathrm{v}} \\ & 0 \leq d_{\mathrm{SH}} \leq 1 & \Delta T_{\mathrm{pinch}} \geq 10 \text{ K} \\ & T_{\mathrm{EG,min}} \geq 120 \text{ °C} & \end{aligned}$$

where P_{evap} and P_{cond} are the evaporating and condensing pressures, d_{SH} is the degree of superheating and $\dot{m}_{\mathrm{wf}}$ is the mass flow rate of working fluid. In Configuration 1, the fraction of the total available jacket water, f_{JW}, used by the ORC engine is also a decision variable. If no jacket water is used, the jacket-water heat exchanger is removed. P_{crit} is the critical pressure and T_3 is the expander inlet temperature, which must remain at or below T_{max}, the maximum allowable temperature for chemical stability given by REFPROP [21]. The working fluid temperature at the expander exit, T_4, is constrained to be at or above that of saturated vapour at the same pressure, $T_{4\mathrm{v}}$, to avoid expansion into the two-phase region. The minimum approach temperature, $\Delta T_{\mathrm{pinch}}$, in each heat exchanger is 10 K or higher. The limit on the

minimum temperature reached by the CHP-ICE exhaust gas, $T_{\mathrm{EG,min}}$, is imposed to avoid condensation. The optimisation problems are solved in MATLAB, using the interior-point algorithm of the *fmincon* optimiser, making use of the *multistart* structure to optimise from different starting points.

The set of seven working fluids considered includes both hydrocarbons and refrigerants, all selected on the basis of low global warming potential and ozone depletion potential. Evidently many more fluids exist than could be studied here, hence fluids which are commonly proposed for CHP-ICE applications are chosen.

2.3.2. Application fit and working fluid selection

A simplified model is used during the early design phase to account for the building demand for hot water over the course of a year. In this model, the building requires the full amount of CHP-ICE heat for a given fraction of the year. During this period, the building demand takes precedence and the jacket-water heat is diverted to the building rather than to the ORC engine in Configuration 1. The exhaust gas heat (which is routed only to the ORC evaporator) must be replaced by burning natural gas in hot-water boilers. At all other times there is excess heat and the ORC engine is able to extract the optimal amount of heat without penalty. The building heating demand is therefore aggregated into a single parameter. The ORC engine in Configuration 2 ultimately delivers all CHP-ICE heat from both the exhaust gas and the jacket water to the building but is expected to deliver reduced electrical power because of the higher condensing temperature.

The simplified model is evidently unable to capture the full effects of different heat demand profiles on the ORC engine performance. However, the model allows a preliminary study of the impact of the building thermal demand on the project's profitability. At this stage of the design, the CHP-ICE is assumed to run at full-load whenever it is active, as part-load ORC performance curves are not yet available. The cycle designs and working fluids that deliver the shortest discounted payback period are selected for Configurations 1 and 2. While this does not necessarily coincide with the maximum NPV of the project, the DPP is a widely-used and intuitive metric for such projects.

2.3.3. Detailed ORC engine design

With the cycle and working fluid established, the sizes of the heat exchangers are fixed for use in subsequent simulations. An expander design that maximises the net power output for the chosen cycle is identified by means of the optimisation approach described in Section 2.1.2. Again, the geometry and valve timings of this component are fixed for the remainder of the analysis.

2.3.4. Part-load simulation

For the part-load simulation, it is first necessary to establish the ORC power output for the range of part-load operating points of the CHP-ICE. Each of these operating points corresponds to a different exhaust gas temperature and mass flow rate, creating a need to optimise the cycle of the ORC engine for each point. The objective function to be maximised here is the net power output, as the cost of the system has already been set in the initial design. While constraining the heat exchanger and expander geometries to equal those

of the full-load design, the mass flow rate, cycle pressure ratio and working-fluid superheat at the expander inlet are all allowed to vary in order to deliver the maximum power output for each condition. The remaining constraints described in Section 2.3.1 are also applied. This process leads to a part-load power output curve for the ORC system, spanning the operating range of the CHP-ICE.

2.3.5. Application-specific ORC engine performance

Once an ORC design and working fluid has been identified, and its part-load performance calculated, we assess the time-varying electricity and heating demand for particular buildings and the effect on the different ORC engine configurations. The CHP-ICE operating point is optimised to meet the building electrical demand with the CHP-ICE and ORC output at least cost, also factoring in time-varying grid electricity and gas prices. It is also possible to operate CHP-ICE units in heat-led operation, whereby the unit ramps up and down to meet the building heat requirement, but this is less prevalent in the types of commercial buildings considered in this study.

The study is carried out on a year's worth of building data and utility prices, supplied by a major national supermarket. Heating and electricity consumption profiles are used for thirty buildings at half-hourly resolution, with retail floor areas of 1900 – 5600 m^2. The approach followed is discussed in greater detail in Le Brun et al. [40]. The average heat-to-power ratios of the buildings ranges from 0.21 to 0.96, with a mean of 0.54, indicating that the average electrical demand exceeds heat demand in all cases, often by a considerable margin.

The benefit derived from the ORC engine is measured in terms of the reduction (or increase) in the building running costs, as the primary effect of the ORC engine is to reduce slightly the quantity of natural gas required to deliver the optimum amount of electricity to the building. The running cost savings are then expressed in terms of DPP and NPV for reporting purposes. Benefits arising from eligibility for the CHPQA scheme are not factored into the stated project returns, and would represent additional added value for the building operator where applicable.

3. Results and discussion

The following sections present observations from throughout the design process, with reference to working fluid selection, part-load performance, and project economic metrics.

3.1. Screening phase

The net output power from the ORC engines and the SIC of the installations are shown in Figs. 2 and 3, respectively, optimised for maximum power output. In Configuration 1, some or all of the CHP-ICE jacket water is considered to be available for ORC engine use to preheat the working fluid prior to the evaporator, though most optimal designs use less than half. As the hot water is at a much lower temperature than the exhaust gases but has a high specific heat capacity, full exploitation of the hot water supply by the ORC

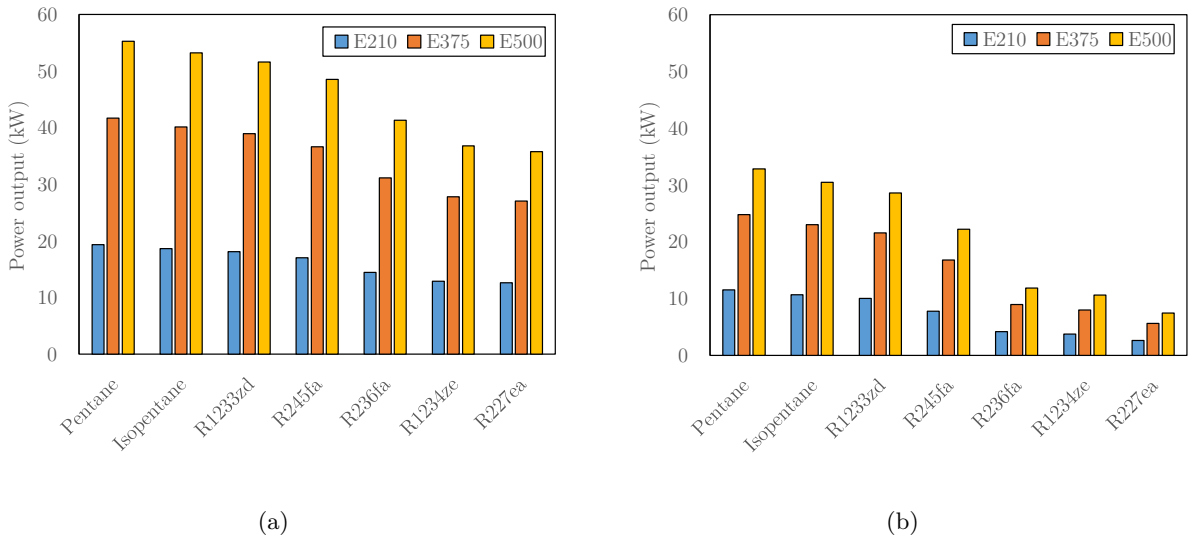

Figure 2: ORC engine net power output, optimised for maximum power with a range of working fluids, in: (a) Configuration 1, and (b) Configuration 2, for three CHP-ICEs at different scales.

system in Configuration 1 means a high working fluid mass flow rate, limiting the expander inlet temperature and hence the system efficiency. Pentane is seen to deliver the highest power output for Configuration 1, but also has the highest SIC of 2350 £/kW when power is maximised. For the E375 engine with pentane, the ORC engine achieves a net efficiency of 14.4% due to the high temperature of the exhaust gas. The maximum amount of heat is extracted from the exhaust gas, as well as 32% of the jacket-water heat, in order to achieve an output power of 41.7 kW.

The ORC engine in Configuration 2 is arranged to reject heat to the building hot water supply, while the CHP-ICE jacket water is also used to generate building hot water. In this configuration, the maximum power outputs are considerably lower than for Configuration 1, a consequence of the higher condensing temperature. This has the effect of reducing the cycle temperature range and therefore the maximum efficiency attainable. The effect is seen to be particularly severe for the refrigerants R236fa, R1234ze and R227ea, which have low maximum temperature limits and require condenser pressures above 10 bar to reject heat to the hot water. Taken together, these factors cause the achievable cycle pressure ratio to be less than 2 for these fluids. The net power output, and consequently the specific investment cost, both suffer as a result of the high back work ratio, as the pump consumes a significant proportion of the expander power output. When optimised for maximum power, the highest power output in Configuration 2 is again observed for pentane, which delivers 24.8 kW. Isopentane and R1233zd also perform well, with the latter having the lowest SIC at 1790 £/kW.

Prior to optimising for SIC, the working fluid candidates are down-selected to R1233zd, R245fa, isopentane and pentane, as they are the most promising from a thermodynamic perspective. In Fig. 4, the power outputs of the ORC engines designed for minimum SIC (shown in Fig. 5) with these working fluids are presented. The minimisation of SIC leads to rather lower power outputs for both configurations, as working

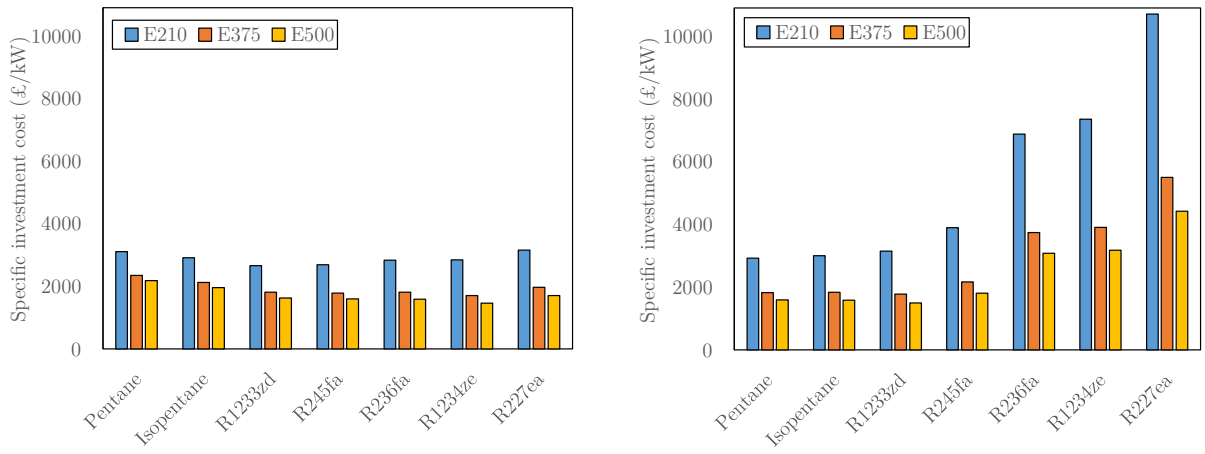

(a) (b)

Figure 3: ORC engine SIC, optimised for maximum power with a range of working fluids, in: (a) Configuration 1, and (b) Configuration 2, for three CHP-ICEs at different scales.

fluid mass flow rates are reduced and temperature differences across the condenser are increased to reduce the heat transfer area requirement. For the E375 CHP-ICE system, the ORC power output ranges from 23.7 kW to 25.8 kW in Configuration 1, and from 16.8 kW to 24.7 kW in Configuration 2.

In both optimisations, the minimum SIC is observed for the ORC system for the largest engine, the E500. This is a consequence of the economies of scale afforded by larger components. The ORC systems for the E210 engine have a markedly higher SIC because a greater proportion of the heat from this CHP engine is delivered in the form of hot water (226 kW) rather than exhaust gas (110 kW). Looking once more at the E375 CHP-ICE, Fig. 5 shows that the lowest SIC occurs for R1233zd in both configurations, at 1600 £/kW and 1750 £/kW respectively. While the total capital cost of the ORC engine for this CHP-ICE and working fluid in Configuration 1 is 9.7% higher than that for Configuration 2, the net power output is 20% higher, producing a lower specific investment cost.

The quantity of jacket-water heat used by the ORC engine in Configuration 1 varies by working fluid, though the usage is universally lower when optimised for minimum SIC rather than maximum power. For the E210 engine with minimum SIC designs, the highest jacket-water utilisation occurs for R245fa, drawing 12.5% of the available jacket-water heat at full-load operation, while R1233zd consumes 9.3% and isopentane just 7.2%. The optimised pentane cycle does not recover any jacket-water heat, instead favouring a lower mass flow rate of working fluid that is heated to high temperature by the exhaust gases. For the E375 and E500 engines, the designs optimised for minimum SIC with all four down-selected working fluids also do not recover any heat from the jacket water, as the marginal cost of the additional jacket-water heat exchanger exceeds the benefit from the additional low-temperature heat input.

The initial thermoeconomic analysis shown in Fig. 5 indicates that the specific investment costs are

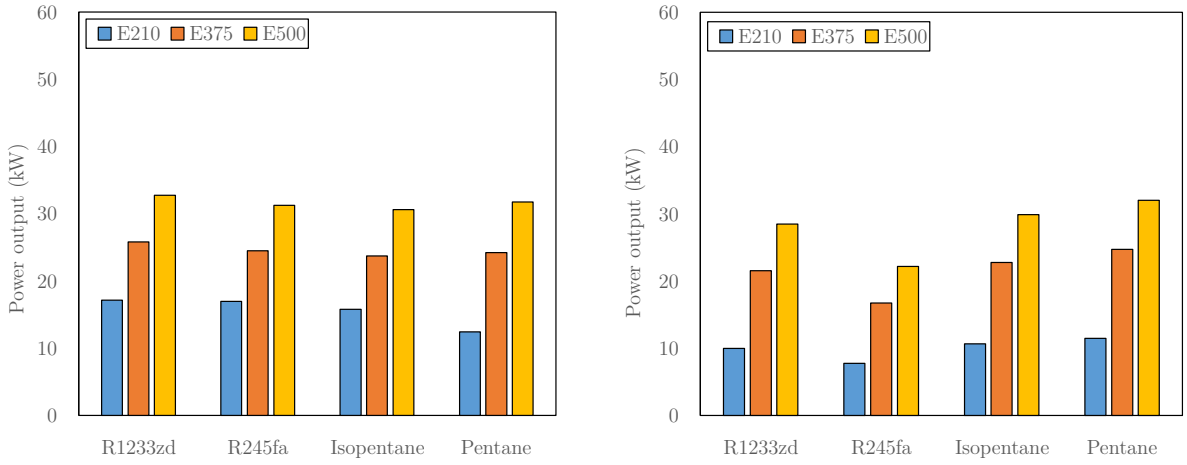

Figure 4: ORC engine net power output, optimised for minimum SIC with a range of working fluids, in: (a) Configuration 1, and (b) Configuration 2, for three CHP-ICEs at different scales.

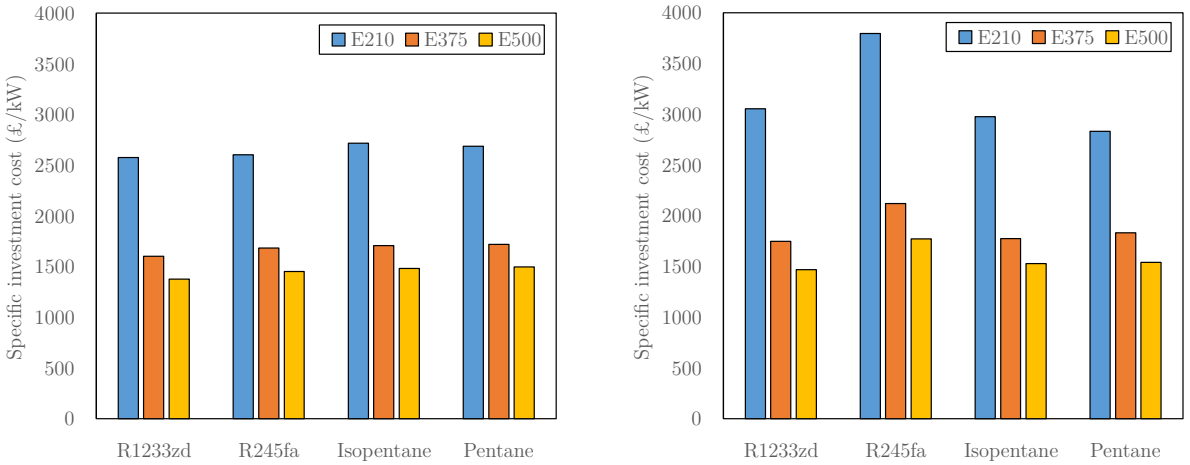

Figure 5: ORC engine SIC, optimised for minimum SIC with a range of working fluids, in: (a) Configuration 1, and (b) Configuration 2, for three CHP-ICEs at different scales.

broadly comparable between all four fluids within each configuration, with the possible exception of R245fa in Configuration 2. R1233zd appears promising, while isopentane and pentane also present as reasonable candidates in both systems. These latter fluids would, however, require additional precautions to manage risks associated with flammability.

The subsequent analysis takes as its starting point the optimum cycle designs for the minimum SIC case for each configuration, as achieving minimum SIC correlates well with minimising the discounted payback period, a commonly-used project viability metric. The E375 CHP-ICE provides the heat source, as it is sized appropriately for the set of buildings to be analysed further in Section 3.4. The findings, however, are expected to be equally applicable to the E210 and E500 CHP-ICE systems.

3.2. Application fit and working fluid selection results

Thus far, the focus has been upon the electrical power output and ORC engine cost. Integration with the building heating requirements is also key, and as such the effect on the project metrics of varying the heat demand is studied early on. At this stage the simplified parametric representation of building heat demand outlined in Section 2.3.2 is employed, in which the annual building heat demand profile is divided into a first portion of the year in which the entire heat output from the CHP is required, and a second portion during which there is assumed to be sufficient heat available to drive the optimised ORC system. Thus, for the first portion, the exhaust gas heat routed to the ORC engine in Configuration 1 must be replaced by burning natural gas in hot-water boilers. This reduces the net savings made from the ORC engine in this configuration.

Fig. 6 shows the discounted payback periods for the two configurations with the four working fluids previously selected. Three scenarios are considered, corresponding to different quantities of building heat demanded. The building model is at this stage deliberately kept generic to study the trade-off between the configurations with broad applicability. The building is considered to require the full heat output from the CHP-ICE (both jacket water and exhaust gas) for 1, 5, and 10% of the year.

The shorter the discounted payback period, the more favourable the project, and so the lowest DPP is evidently of interest. The minimum DPP of 3.0 years occurs for the 1% scenario for Configuration 1 with R1233zd. However, as the building demand for heat rises, the cost of meeting the building need with gas-fired boilers becomes significant. Configuration 2, while delivering less power and offering a higher SIC, has the advantage of delivering all of the CHP-ICE heat to the building hot water supply, either via condenser heat rejection or directly from the jacket water, and thus the economic metrics are unaffected by changes in the heating demand. For the 5% scenario, Configuration 2 is preferable for three out of the four fluids considered, and for the 10% scenario Configuration 2 is preferred for all four. These observations hold whether DPP (Fig. 6) or NPV (Fig. 7) is the metric being used.

While the building heat model used here is a simplified heuristic, and thus far only full-load performance has been considered, it is quickly evident that the trade-off between ORC engine performance and supplying

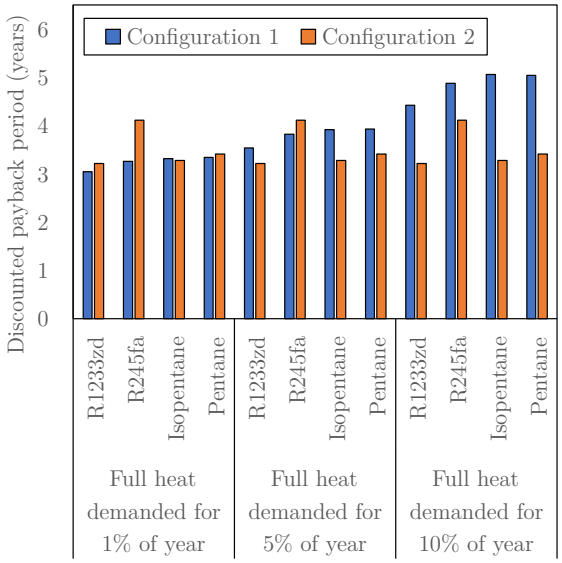

Figure 6: Discounted payback period for each configuration for four working fluids, under different heating demand scenarios. The E375 CHP-ICE provides the exhaust gas heat source.

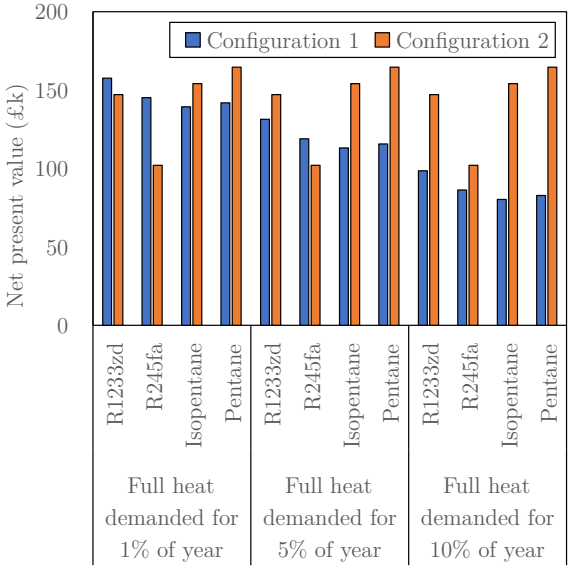

Figure 7: Net present value over 20 years for each configuration for four working fluids, under different heating demand scenarios. The E375 CHP-ICE provides the exhaust gas heat source.

heat to the building rapidly becomes costly if the building has even a modest heat-to-power ratio. In examples where the heat demand is very low, the ORC system arrangement in Configuration 1 presents advantages, but it is likely the economic case for installing the CHP-ICE itself would be much weaker.

Based on the findings in Fig. 6, R1233zd is chosen for the remainder of the analysis, as it consistently enables the lowest DPP across all scenarios and across both configurations, though pentane and isopentane also perform well for Configuration 2.

3.3. Part-load simulation results

To solidify these initial observations, the ongoing analysis seeks to apply a more in-depth simulation approach, drawing on detailed component modelling to produce part-load performance curves. Noting that the cost-optimal ORC engine designs in Configuration 1 for the E375 engine do not draw on the jacket-water heat, and that jacket-water use leads to additional (and likely costly) sensitivity to the building heating demand, the base configuration is amended slightly to draw heat only from the exhaust gas. This both simplifies the system layout and enables additional hot water to be routed directly to the building. This layout is referred to as Configuration 1′ hereafter. The heat from the exhaust gas in Configuration 1′ continues to be available only to the ORC engine, not to the building, in contrast to Configuration 2.

The areas and diameters of the tube-in-tube heat exchangers identified in the full-load optimisation for the E375 engine with R1233zd are shown in Table 2. The evaporator area in each configuration is considerably larger than that of the condenser because of the lower heat transfer coefficient on the exhaust-gas side. Tube-in-tube heat exchangers are typically quite bulky, and thus the designs found would be less suitable for space-constrained applications. In other cases, including the present study, the cost savings can help to justify the footprint of the system.

Table 2: Heat-exchanger designs for the two system configurations for the E375 engine with R1233zd. The diameters quoted are the outer diameters of each pipe. The wall thicknesses of the inner tubes and outer tubes are 3.7 mm and 7.0 mm respectively.

	Configuration 1′		Configuration 2	
	Evaporator	Condenser	Evaporator	Condenser
Area (m^2)	25	3.4	32	9.3
Diameter of inner tube (mm)	65	42	44	46
Diameter of outer tube (mm)	180	109	191	127

In the part-load simulations, the heat exchanger areas and dimensions are constrained to match those identified in the full-load optimisation for minimum SIC, while the geometry and valve timings of the reciprocating-piston expander are fixed by the expander design optimisation, which maximised the power output at full-load CHP-ICE conditions. Alternative optimisation approaches that seek to maximise ORC engine power output across a range of full- and part-load conditions will be investigated in future work.

Table 3 gives the performance of the ORC engines at full and part-load, making use of the more detailed expander model. The net power outputs at full load for the two configurations are 21.8 kW and 20.4 kW respectively, with Configuration 1 delivering 7% higher output. The introduction of the more detailed expander model leads to a slight reduction in the output power for both systems, as the cycle pressure ratio and working-fluid flow rate adjust to accommodate the achievable expander performance.

The expander overall isentropic efficiency in Configuration 1′ at full-load conditions is slightly less than the 70% previously assumed, while the isentropic efficiency obtained for Configuration 2 is slightly higher. The difference in efficiencies is associated with the cycle pressure ratios: at full-load conditions, the expander in Configuration 1′ operates at a design pressure ratio of 7.7, compared to 5.1 for Configuration 2. As the pressure ratio reduces, the throttling losses across the valves are lowered and the isentropic efficiency that can be achieved by an optimised design increases.

At part-load operation, the power generated from the ORC engines decreases, as the CHP-ICE electrical output falls and less heat is delivered to the ORC engine evaporator. However, when the electrical output decreases to 70%, the CHP-ICE heat output decreases by a smaller amount, to 76% of its full-load value. Hence, the heat supply to the ORC engine falls more slowly than the CHP-ICE electrical output. Furthermore, the lower mass flow rate allows for a small improvement in the efficiency of the expander. These effects can be seen in Fig. 8, whereby the ORC engines continue to produce 80 – 83% of their full-load power despite the CHP-ICE operating at 70% electrical output. In both cases, the expander efficiency increases slightly as the heat input, and consequently the mass flow rate of working fluid, decreases. For a fixed-size piston expander, the lower mass flow rate leads to reduced valve losses, particularly at high pressure ratios.

Table 3: Part-load performance of each ORC system configuration, corresponding to different working points of the E375 CHP-ICE. The ORC working fluid is R1233zd. Cycle efficiency is defined relative to the heat available from the CHP-ICE exhaust gas.

	Configuration 1′			Configuration 2		
CHP-ICE output (% of full load)	60	80	100	60	80	100
ORC engine power output (kW)	14.6	19.7	21.8	13.4	18.8	20.4
ORC engine cycle efficiency (%)	9.1	9.9	9.2	8.4	9.5	8.6
Expander overall efficiency (%)	69.9	68.7	66.6	74.0	72.9	72.5

For the subsequent application-specific work, a polynomial fit of the form $y = ax^2 + bx + c$ is fitted to the set of five part-load simulations for each configuration shown in Fig. 8 and found to replicate the simulated power output to within 3%. For Configuration 1′, the curve is defined by $a = -0.0134$, $b = 2.93$ and $c = -60.1$, while for Configuration 2, the values are found to be $a = -0.0219$, $b = 4.29$ and $c = -112$.

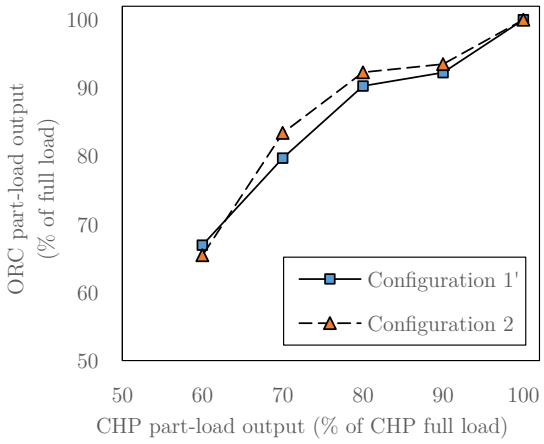

Figure 8: Part-load net power output for each ORC engine configuration as a function of CHP-ICE (E375) part-load percentage.

3.4. Application-specific ORC engine performance results

To assess the ORC system performance robustly, the proposed designs are simulated within a half-hourly building model, drawing on historical data for gas and electricity consumption and utility prices from 2017-2018. An example of the building electricity and heating demand is shown in Fig. 9, for a week in winter. At full load, the CHP-ICE produces a total heat output that slightly exceeds its electrical output, while the building electricity demand exceeds the heating demand by 72% for the period shown. Winter operation represents a high heat demand case: at other times of year the electricity demand for the same building can be up to five times the heating demand, thus ensuring ample scope for waste heat recovery for the ORC system.

The simulated output power for both configurations are shown in Fig. 10 for the same week. Configuration 1′ shows a higher power output, as expected. The CHP-ICE and ORC engine run almost continuously to supply the building needs, with the CHP-ICE operating at full power output for 21% of the period shown. A similar analysis of a week in summer shows an even higher proportion, with the CHP-ICE at full load for 33% of the week in order to cover the refrigeration loads.

The operating cost savings over a year are shown for each of the thirty buildings in Fig. 11, plotted against the buildings' heat-to-power ratio. It is immediately clear that the two configurations perform very differently. The cost savings depend strongly on the building heat-to-power ratio for Configuration 1′, as indicated by the preliminary analysis in Section 3.2. Positive savings are seen for buildings with heat-to-power ratios below around 0.6, though it is only for the lowest heat-to-power ratio building, at 0.21, that the cost savings exceed those of Configuration 2. The latter configuration shows consistent cost savings in the range of £10,000 – £18,000 across all of the buildings thanks to its ability to deliver all of the CHP-ICE heat to meet heating demands. The slightly reduced power output and cycle efficiency of Configuration 2 are more than offset by the ability to use both jacket water and exhaust gas heat to meet building heating requirements during periods of high demand, while additional costs are incurred for natural gas heating to

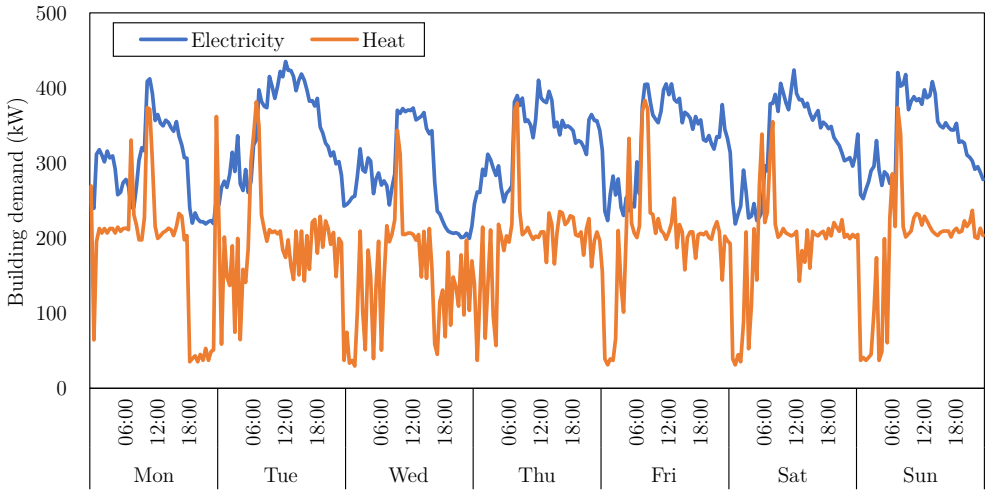

Figure 9: Example time-history of building electricity and heating demand over the course of a week in winter.

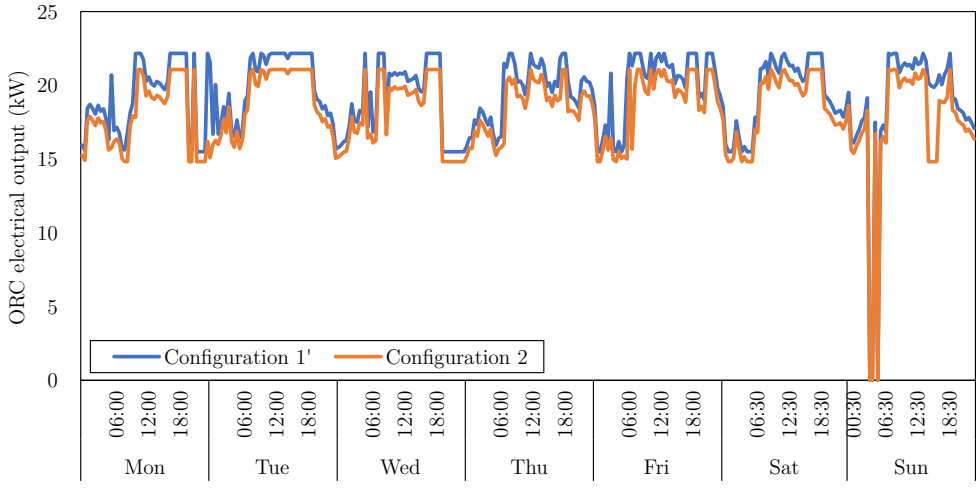

Figure 10: ORC net power output for each configuration over the course of a week in winter.

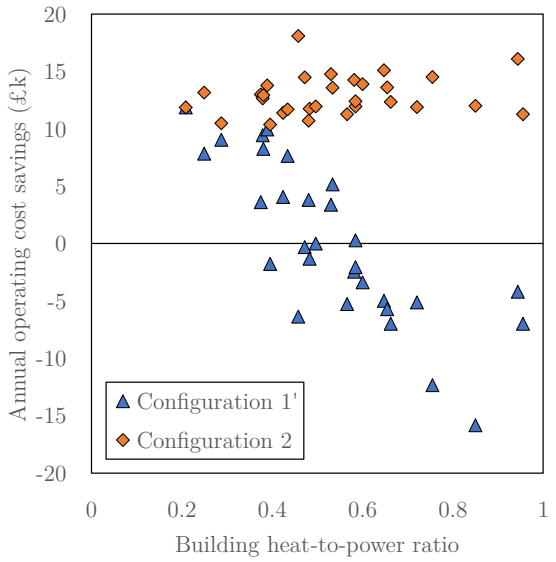

Figure 11: Operational cost savings for ORC engine in Configurations 1′ and 2 for the set of thirty buildings, plotted against the heat-to-power ratio of each building.

make up the shortfall from providing jacket-water heat alone to the building in Configuration 1′.

Fig. 11 also makes clear the range of building heat-to-power ratios captured within the data set of historical electricity and heating demand profiles (0.21 to 0.96). The conclusions are seen to hold across a range of scales, from 210 to 500 kW of CHP-ICE electrical output. The robustness of the observations made across a variety of building profiles and sizes gives confidence that the findings made here are applicable to a wide range of energy-intensive buildings where average electricity demand exceeds average heating demand, for which UK supermarkets are one example.

The project viability metrics are shown in Figs. 12 and 13, with the buildings ordered by increasing heat-to-power demand ratio. The discounted payback periods for Configuration 1′ vary widely, and in many cases the project does not pay back the initial investment. The DPP is therefore not defined, which is signified in Fig. 12 by the absence of a bar for that building. For Configuration 2, the discounted payback periods range from 3.5 to 7.5 years, with an average of 5.6 years. As a standalone economic decision, these payback periods are likely to bring installation of the ORC system close to viability, though the DPP thresholds vary by company and by industry.

Net present values also vary widely for Configuration 1′, from –£264k to a maximum of £55k. It is evident that the configuration has only limited applicability among the types of buildings considered, achieving a positive NPV in just seven cases out of thirty. Of the buildings which do show a positive NPV, the highest heat-to-power ratio is 0.43. Configuration 2 shows a much more robust performance, with NPVs ranging from £45k to £134k. The ability to provide economic benefits to all thirty buildings with a single ORC system design is encouraging, as this could pave the way for larger manufacturing volumes of small-scale

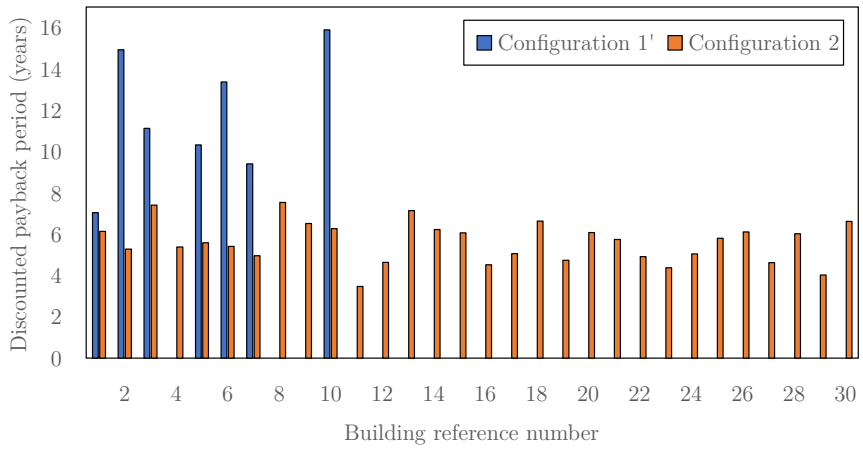

Figure 12: Discounted payback period for each ORC engine configuration for the set of thirty buildings, arranged from lowest to highest heat-to-power ratio. Where no bar is shown, the project does not recoup its costs and the DPP is not defined.

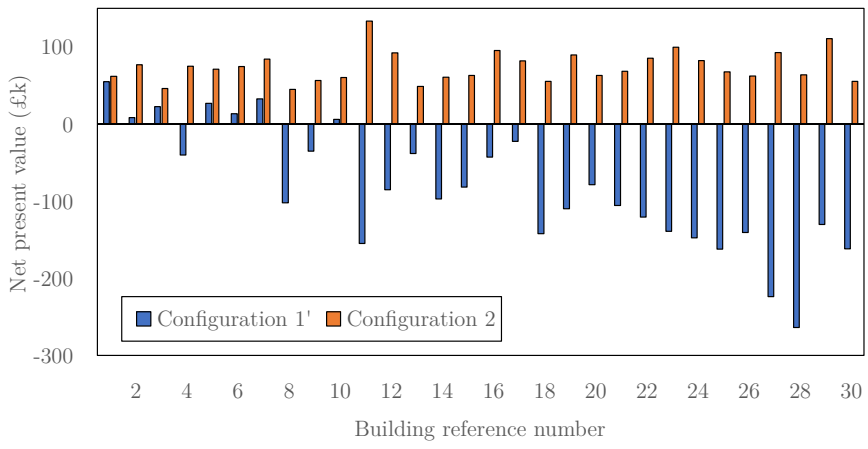

Figure 13: Net present value over twenty years for each ORC engine configuration for the set of thirty buildings, arranged from lowest to highest heat-to-power ratio.

ORC systems than has been possible to date. At present, the one-off nature of most ORC engine installations means that small systems (e.g., below 100 kW) are rarely cost-effective, as considerable engineering costs are incurred to specify each installation. Identification of a common design configuration could also lead to reduced costs for integration of the ORC engine with the CHP-ICE, by standardising the connections required.

4. Conclusions

Driven to lower both the cost and climate impact of the energy they use, large supermarket chains and operators of similarly energy-intensive buildings are investigating the benefits of small-scale CHP systems based on internal combustion engines (ICE). However, the low heat-to-power ratio of the buildings causes a poor fit to the CHP output, leading to longer payback periods and risking non-compliance with the CHP Quality Assurance programme.

ORC engines, operating in bottoming cycle configuration, offer the potential to address this issue by converting the unused heat to power. A modelling framework has therefore been presented by which prospective CHP-ORC configurations can be assessed. The approach has been used to evaluate two possible configurations for ORC engines. Both configurations recover heat from the exhaust gases of the engines, and exploit the high temperatures available from doing so. In Configuration 1, an additional quantity of heat can be recovered from the jacket water of the CHP-ICE to increase the ORC engine power output. In Configuration 2, the ORC condensing temperature is increased, which prevents heat recovery from the jacket water, but allows the ORC system to provide hot water at 70 °C for building heating purposes. The former promises improved performance at design conditions, while the latter ensures that all heat from the CHP-ICE is available to meet spikes in the building heat demand.

The design power output and specific investment costs have been identified for systems optimised for maximum power and minimum SIC. For a 375-kWe CHP-ICE, a system configured for maximum power achieves 41.7 kW in Configuration 1, with pentane as the working fluid, while the peak power for Configuration 2 is 24.8 kW with the same fluid. When optimising for minimum SIC with the same CHP-ICE, the maximum power outputs are rather closer, at 25.8 kW and 24.7 kW for Configuration 1 with R1233zd and Configuration 2 with pentane, respectively. The lowest SICs are obtained for both configurations when using R1233zd as the working fluid: Configuration 1 costs 1600 £/kW while Configuration 2 costs 1750 £/kW. Configuration 2 therefore performs less well than Configuration 1 in both power output and SIC, as a consequence of the elevated condensing temperature required to reject heat to the building supply.

Using a stylised building heat demand model, the effect of delivering CHP-ICE heat to the ORC engine in Configuration 1 is investigated, through project metrics such as discounted payback period and net present value. A high level of sensitivity to the building heat demand is observed, with noticeable deterioration in project benefits even at low heating demand levels. The ORC engine in Configuration 2 is capable of

delivering all of the CHP-ICE heat to the building at the required temperature, decoupling its economic performance from the building heat requirements.

The finding is borne out in the subsequent in-depth analysis, making use of component models for the heat exchangers and the reciprocating-piston expander to predict the part-load performance of the ORC engine. Simulating the ORC engine operation over a year for a wide-ranging dataset of thirty different supermarkets across the UK shows that the operating cost savings in Configuration $1'$ rapidly become negative as the building heat-to-power ratio increases, with no projects viable above a heat-to-power ratio of 0.43. For this configuration, heating requirements are therefore a major determinant of the ORC system benefits, and only a small subset of the buildings would offer viable projects. Configuration 2, by contrast, delivers consistent benefits across the range of buildings studied, with discounted payback periods between 3.5 and 7.5 years and net present values between £45k and £134k. This configuration therefore appears to offer attractive possibilities for larger-volume manufacture than has previously been possible. This is an important finding, with implications for large supermarket chains and a wide variety of other energy-intensive buildings, as well as for ORC manufacturers and installers seeking to standardise and mass-produce their designs.

5. Acknowledgements

This work was supported by the UK Engineering and Physical Sciences Research Council [grant number EP/P004709/1, and award numbers 1855524 and 1855813]. The authors would also like to thank the Imperial College President's PhD Scholarship Scheme, and the Climate-KIC PhD Added Programme for funding this research. The support of Sainsbury's Supermarkets Ltd in providing a dataset on energy-intensive buildings is also gratefully acknowledged. Data supporting this publication can be obtained on request from cep-lab@imperial.ac.uk.

References

[1] M. C. Simpson, M. A. Chatzopoulou, O. A. Oyewunmi, C. N. Markides, Technoeconomic analysis of internal combustion engine - organic Rankine cycle cogeneration systems in energy-intensive buildings, Energy Procedia 158 (2019) 2354–2359. doi:10.1016/j.egypro.2019.01.283.

[2] C. N. Markides, The role of pumped and waste heat technologies in a high-efficiency sustainable energy future for the UK, Applied Thermal Engineering 53 (2) (2013) 197–209. doi:10.1016/j.applthermaleng.2012.02.037.

[3] Department for Business, Energy & Industrial Strategy, The CHPQA Standard Issue 7 (2018). URL https://assets.publishing.service.gov.uk/government/uploads/system/uploads/attachment_data/file/765578/CHPQA_Standard_Issue_7.pdf

[4] C. N. Markides, Low-concentration solar-power systems based on organic Rankine cycles for distributed-scale applications: Overview and further developments, Frontiers in Energy Research 3 (2015) 47. doi:10.3389/fenrg.2015.00047.

[5] J. Freeman, K. Hellgardt, C. N. Markides, An assessment of solar-powered organic Rankine cycle systems for combined heating and power in UK domestic applications, Applied Energy 138 (2015) 605–620. doi:10.1016/j.apenergy.2014.10.035.

[6] J. Freeman, K. Hellgardt, C. N. Markides, Working fluid selection and electrical performance optimisation of a domestic solar-ORC combined heat and power system for year-round operation in the UK, Applied Energy 186 (2017) 291–303. doi:10.1016/j.apenergy.2016.04.041.

[7] O. Oyewunmi, C. Markides, Thermo-economic and heat transfer optimization of working-fluid mixtures in a low-temperature organic Rankine cycle system, Energies 9 (6) (2016) 448. doi:10.3390/en9060448.

[8] D. Maraver, J. Royo, V. Lemort, S. Quoilin, Systematic optimization of subcritical and transcritical organic Rankine cycles (ORCs) constrained by technical parameters in multiple applications, Applied Energy 117 (2014) 11–29. doi:10.1016/j.apenergy.2013.11.076.

[9] M. Lampe, J. Groß, A. Bardow, Simultaneous process and working fluid optimisation for Organic Rankine Cycles (ORC) using PC-SAFT, Computer Aided Chemical Engineering 30 (2012) 572–576. doi:10.1016/B978-0-444-59519-5.50115-5.

[10] M. T. White, O. A. Oyewunmi, A. J. Haslam, C. N. Markides, Industrial waste-heat recovery through integrated computer-aided working-fluid and ORC system optimisation using SAFT-γ Mie, Energy Conversion and Management 150 (2017) 851–869. doi:10.1016/j.enconman.2017.03.048.

[11] O. A. Oyewunmi, A. I. Taleb, A. J. Haslam, C. N. Markides, An assessment of working-fluid mixtures using SAFT-VR Mie for use in organic Rankine cycle systems for waste-heat recovery, Computational Thermal Sciences: An International Journal 6 (4) (2014) 301–316. doi:10.1615/.2014011116.

[12] M. T. White, O. A. Oyewunmi, M. A. Chatzopoulou, A. M. Pantaleo, A. J. Haslam, C. N. Markides, Computer-aided working-fluid design, thermodynamic optimisation and thermoeconomic assessment of ORC systems for waste-heat recovery, Energy 161 (2018) 1181–1198. doi:10.1016/j.energy.2018.07.098.

[13] L. M. T. van Kleef, O. A. Oyewunmi, C. N. Markides, Multi-objective thermo-economic optimization of organic Rankine cycle (ORC) power systems in waste-heat recovery applications using computer-aided molecular design techniques, Applied Energy (2019) to appear.

[14] S. Lecompte, H. Huisseune, M. van den Broek, S. De Schampheleire, M. De Paepe, Part load based thermo-economic optimization of the Organic Rankine Cycle (ORC) applied to a combined heat and power (CHP) system, Applied Energy 111 (2013) 871–881. doi:10.1016/j.apenergy.2013.06.043.

[15] G. Shu, G. Yu, H. Tian, H. Wei, X. Liang, Z. Huang, Multi-approach evaluations of a cascade-Organic Rankine Cycle (C-ORC) system driven by diesel engine waste heat: Part A Thermodynamic evaluations, Energy Conversion and Management 108 (2016) 579–595. doi:10.1016/j.enconman.2015.10.084.

[16] R. Turton, R. C. Bailie, W. B. Whiting, J. A. Shaeiwitz, Analysis, Synthesis and Design of Chemical Processes, Prentice Hall International Series in the Physical and Chemical Engineering Sciences, Pearson Education, 2008.

[17] K. Braimakis, S. Karellas, Integrated thermoeconomic optimization of standard and regenerative ORC for different heat source types and capacities, Energy 121 (2017) 570–598. doi:10.1016/j.energy.2017.01.042.

[18] M. S. Peters, K. D. Timmerhaus, R. E. West, Plant design and economics for chemical engineers, Vol. 4, McGraw-Hill New York, 1968.

[19] Ener-G, Ener-G cogeneration (2016).
URL www.energ-group.com/combined-heat-and-power/cogeneration

[20] O. A. Oyewunmi, C. J. Kirmse, A. M. Pantaleo, C. N. Markides, Performance of working-fluid mixtures in ORC-CHP systems for different heat-demand segments and heat-recovery temperature levels, Energy Conversion and Management 148 (2017) 1508–1524. doi:10.1016/j.enconman.2017.05.078.

[21] E. Lemmon, M. Huber, M. McLinden, Reference fluid thermodynamic and transport properties - Refprop 9.1 (2013).
URL https://www.nist.gov/sites/default/files/documents/srd/REFPROP9.PDF

[22] O. A. Oyewunmi, A. I. Taleb, A. J. Haslam, C. N. Markides, On the use of SAFT-VR Mie for assessing large-glide fluorocarbon working-fluid mixtures in organic Rankine cycles, Applied Energy 163 (2016) 263–282. doi:10.1016/j.apenergy.2015.10.040.

[23] I. Vaja, A. Gambarotta, Internal combustion engine (ICE) bottoming with organic Rankine cycles (ORCs), Energy 35 (2) (2010) 1084–1093. doi:10.1016/j.energy.2009.06.001.

[24] W. H. McAdams, Heat Transmission, 2nd Edition, McGraw-Hill, New York-London, 1942.

[25] J. C. Chen, Correlation for boiling heat transfer to saturated fluids in convective flow, Industrial and Engineering Chemistry Process Design and Development 5 (3) (1966) 322–329. doi:10.1021/i260019a023.

[26] G. Hewitt, G. Shires, T. Bott, Process heat transfer, CRC Press, 1994.

[27] M. M. Shah, A general correlation for heat transfer during film condensation inside pipes, International Journal of Heat and Mass Transfer 22 (4) (1979) 547–556. doi:10.1016/0017-9310(79)90058-9.

[28] M. A. Chatzopoulou, M. Simpson, P. Sapin, C. N. Markides, Off-design optimisation of organic Rankine cycle (ORC) engines with piston expanders for medium-scale combined heat and power applications, Applied Energy 238 (2019) 1211–1236. doi:10.1016/j.apenergy.2018.12.086.

[29] M. A. Chatzopoulou, C. N. Markides, Thermodynamic optimisation of a high-electrical efficiency integrated internal combustion engine - Organic Rankine cycle combined heat and power system, Applied Energy 226 (2018) 1229–1251. doi:10.1016/j.apenergy.2018.06.022.

[30] J. Bao, L. Zhao, A review of working fluid and expander selections for organic Rankine cycle, Renewable and Sustainable Energy Reviews 24 (2013) 325–342. doi:10.1016/j.rser.2013.03.040.

[31] M. C. Simpson, P. Sapin, C. Kirmse, G. Rotolo, P. De Palma, C. N. Markides, Assessment of reciprocating-piston and screw expanders for waste-heat recovery applications, in: UK Heat Transfer Conference, London, UK, 2017.

[32] P. Sapin, M. C. Simpson, A. J. White, C. N. Markides, Lumped dynamic analysis and design of a high-performance reciprocating-piston expander, in: International Conference on Efficiency, Cost, Optimisation, Simulation and Environmental Impact of Energy Systems, San Diego, CA, 2017.

[33] J. Heywood, Internal Combustion Engine Fundamentals, McGraw-Hill Education, 1988.

[34] P. J. Shayler, D. K. W. Leong, M. Murphy, Friction teardown data from motored engine tests on light duty automotive diesel engines at low temperatures and speeds, in: Fall Technical Conference of the ASME Internal Combustion Engine Division, Erie, Pennsylvania, 2003, pp. 1–18.

[35] U. Lekic, Fluid flow and heat transfer in a helium gas spring-computational fluid dynamics and experiments, Ph.D. thesis, University of Twente (2011).
URL http://doc.utwente.nl/78498/1/thesis{_}U{_}Lekic.pdf

[36] C. D. Rakopoulos, G. M. Kosmadakis, A. M. Dimaratos, E. G. Pariotis, Investigating the effect of crevice flow on internal combustion engines using a new simple crevice model implemented in a CFD code, Applied Energy 88 (1) (2011) 111–126. doi:10.1016/j.apenergy.2010.07.012.

[37] J. Müller, C. A. Shoemaker, Influence of ensemble surrogate models and sampling strategy on the solution quality of algorithms for computationally expensive black-box global optimization problems, Journal of Global Optimization 60 (2) (2014) 123–144. doi:10.1007/s10898-014-0184-0.

[38] W. D. Seider, D. R. Lewin, J. D. Seader, S. Widagdo, R. Gani, K. M. Ng, Product and process design principles : synthesis, analysis, and evaluation, John Wiley & Sons Inc., New York, 2017.

[39] AREA, AREA product catalogue (2017).
URL http://www.areacooling.co.uk/?download=true{#}otro

[40] N. Le Brun, S. Acha, M. Simpson, N. Shah, C. N. Markides, Financial prospects for small-scale stationary ORC-ICE CHP (200-500 kWe ICE): the case of the UK food retail sector, in preparation.